Battery-Less Short-Term Smoothing of Photovoltaic Generation Using Sky Camera

Mojtaba Saleh, *Student Member, IEEE*, Lindsay Meek, *Member, IEEE*, Mohammad A. S. Masoum, *Senior Member, IEEE*, and Masoud Abshar

***Abstract*—There is a growing concern over addressing the adverse effects of variations in the output power of distributed generators such as photovoltaic generation (PVG) systems that continue to be widely introduced into power networks. Nowadays, most network operators are requiring these intermittent energy resources to seek compliance with new regulations pertaining to the restriction of their export power fluctuations. This paper aims to investigate the smoothing of the export power fluctuations primarily attributed to clouds passing over the PVG plant, which are traditionally compensated by integrating a battery storage (BS) system. The idea of incorporating short-term solar prediction information into the conventional smoothing approach is examined to indicate how it affects the engagement of BS in the smoothing process. Afterward, an enhanced solar forecasting scheme based on whole-sky imaging is proposed and its performance is demonstrated through several real-time experiments complemented with simulation studies. The results reveal that the proposed PVG smoothing strategy is capable of successfully filtering rapid export power fluctuations to an acceptable extent and the conventional generation reserves will experience a negligible amount of remaining undesired power variation. This clearly bears out the hypothesis of battery-less PVG regulation.**

***Index Terms*—Cloud forecasting, photovoltaic systems, power smoothing, sky camera imaging.**

I. Introduction

THE escalating deployment level of photovoltaic generation (PVG) systems and their growing contribution to meet the increasing energy demand has created emerging issues in the power systems planned to operate with conventional generation resources. The uncertainty of PVG, which is primarily attributed to clouds obscuring the sun and substantial insolation variations can lead to an extra burden on the conventional operational reserve of the power system, in terms of the incidence of operation as well as required capacity [1]. This gives rise to a critical necessity for associated regulations on ramp rate (RR) of the variations in photovoltaic (PV) and wind generations, e.g., 10% of plant's rated capacity per minute is widely adopted by utility operators [2]–[4]. As an immediate solution, different energy storage technologies have been proposed and applied to address the intermittency of PVG, i.e., battery storage (BS) [5]–[10], ultra-capacitors [11], [12], superconducting magnetic energy storage [13], [14], fuel cells [15], and flywheels [16]. Among these technologies, BS-based solutions have become more prevalent due to recent improvements in performance, declining trend in the cost, wide power range, and scalable capacity. Essentially, the backup storage system reacts to the erratic fluctuations in the PV export power termed as a *reactive* smoothing approach. Therefore, sufficient storage capacity proportional to the magnitude of the sudden PVG variations is required for a proper smoothing treatment. This also substantially raises the capital cost of the PVG system and consequently the generation cost of the solar electricity. On the other hand, the solar irradiance forecasting and projected generation information of the PV facilities enable a predictive approach, which initiates the ramp down function sufficiently prior to the passing clouds shade the PV arrays. Therefore, upon the incidence of the shading event, the PV plant will not experience any severe fluctuation. This solution, termed as *proactive*, significantly shrinks the required smoothing backup. Moreover, solar irradiance prediction approaches could offer remarkable reliability and power quality advantages to the power system, i.e., serve to improve the ability to dispatch utility-scale PV plants, enabling less variable PVG in urban feeders and alleviate the operation of voltage regulation equipment, and allow efficient and smart control of storage systems integrated into PV plants. There is a wide range of solar forecasting methods available; typically they differ in the temporal and spatial domain. Those range from a very short-term time frame of one minute to a full day ahead, with a spatial accuracy ranging from very coarse 50 km down to a more precise 1 km domain. Ground-based cloud imagery approaches offer comparatively higher resolutions in both the temporal and spatial domains, making them good candidates for PVG smoothing applications that require identifying rapid irradiance variations [17]. There are a series of publications available on solar irradiance forecasting [18]–[22], which to some extent describe the fundamentals. The acquired

Manuscript received November 15, 2016; revised August 10, 2017; accepted September 15, 2017. Date of publication October 27, 2017; date of current version February 1, 2018. This work of M. Saleh was supported by a Curtin International Postgraduate Research Scholarship (CIPRS), which was sponsored by Magellan Powertronics. Paper no. TII-16-1373. *(Corresponding author: Mojtaba Saleh.)*

M. Saleh and M. A. S. Masoum are with the Centre for Smart Grid and Sustainable Power Systems, Department of Electrical Engineering, Curtin University, Perth, WA 6102, Australia (e-mail: mojtaba_saleh@hotmail.com; m.masoum@curtin.edu.au).

L. Meek and M. Abshar are with the Magellan Powertronics Pty Ltd, Perth, WA 6163, Australia (e-mail: lmeek@magellanpower.com.au; mabshar@magellanpower.com.au).

Color versions of one or more of the figures in this paper are available online at http://ieeexplore.ieee.org.

Digital Object Identifier 10.1109/TII.2017.2767038

image is first captured by a whole-sky camera and transformed into a red-to-blue-ratio (RBR) image. Then, it is compared with a corresponding reference image of the clear sky, where the difference in RBR values is used to distinguish cloud regions. This is then processed to generate a cloud map, which in conjunction with the cloud base height information yields a ground shadow map with a range of up to 5 km from the observation spot [18]–[20]. West *et al.* [21], have deployed an artificial neural network to make an estimation on the respective cloudiness degree of each pixel while Bernecker *et al.* [22] proposed a fixed value RBR segmentation approach augmented by cloud texture filters. Another key element investigated in different approaches is the cloud motion, i.e., the cross-correlation of consecutive images[18]–[20] and dense optical flow [21] as well as a non-rigid registration method which takes the local deformation of clouds into account [22]. The insolation level is conclusively predicted according to the present cloud regions and their prevailing movements. In a traditional method as used by [18]–[20], the present cloud map is advected by extrapolating the observed cloud motion elements to identify a projected cloud map and then by means of ray-tracing method a shadow map is calculated. However, [21] correlates the occlusion of the sun to the cloudiness figure of an annulus area with radii proportional to the forecast range. Bernecker *et al.* [22], have defined and examined an area in which the clouds have a potential of obscuring the sun to generate an occlusion probability that is used to estimate the projected insolation level. Aside from the inherent inaccuracies arising from the cloud formation and evaporation, the perspective error, and the limited field of view, the extensive evaluative results presented in [20] implies an inconsistency in the incidence and magnitude of erroneous predictions from day to day. These inconsistencies call for a more robust and improved solution.

In this paper, an averaged cloud prediction approach is proposed that considers multiple historical observations to obtain a single projected cloud region. Furthermore, this method is applied to generate a series of equally spaced prediction information to improve the robustness while addressing the occasional inaccuracies of the algorithm in the identification of shape, dimensions, or motion of clouds. Ultimately, the cloud prediction information is incorporated into the conventional PVG regulation algorithm as an early warning of the upcoming shading events, which starts the export ramp down to a reduced level so that it is not affected by the passing clouds.

The main contribution of this paper is a practical predictive solution addressing the short-term intermittency of the solar power to meet the RR regulations mandated by the utility grid operators. The experimental results confirm that the proposed approach effectively minimises the amount of required backup capacity, which is tightly restricted to a certain level. Utility grid operators normally allow for the low amplitude generation variations to be accommodated by the existing spinning reserve capacity. This proves the hypothesis of a battery-less solution to the short-term PVG regulation in practice.

The remainder of the paper is organised into five sections. Sections II and III present the proposed imagery cloud prediction algorithm, and a detailed explanation on different cloud prediction-based smoothing approaches, respectively; followed the developed experimental testbed is described in Section IV. The performances of several smoothing techniques are comparatively surveyed through experimental measurements and simulation studies in Section V, followed by the conclusion.

II. Proposed Averaged Cloud Prediction Algorithm

The cloud prediction procedure is primarily an image processing operation, which considers successive whole sky images captured by a fish-eye camera and generates projected cloudiness figures, which are interpreted as a reliable indication of projected PVG power ramp downs. In this section, the major contribution is a multitarget prediction technique that examines cloud prediction information associated with a series of prediction instants within a prediction range of interest. This allows an averaged prediction that improves the overall performance of the algorithm in terms of robustness and accuracy.

A. Correcting Lens Distortion

Fish-eye lens produces an extremely wide field of view while the optical distortion is typical of the fish-eye images. For the purpose of motion analysis, the spherical perspective is projected onto the flat plane using the OCamCalib calibration toolbox [23]. The toolbox processes multiple sample photos of a chessboard template and obtains the coordinates of all corners and then calculates the corresponding inherent optical characteristics of the lens. Then, a mapping lookup array is generated for instant conversion of the fish-eye hemispherical view into an undistorted image. The fish-eye lens normally creates a compressed artifact toward the periphery of the image. The calibration process is also significantly erroneous in marginal coordinates due to the nonlinear characteristics of the lens toward the rim. Hence, the undistortion is conducted so that the poorly undistorted region with higher circular angle is projected outside the destination frame. This can be achieved by adjusting the projection factor F_p in the OcamCalib toolbox to ignore the calibration error at the price of limited view angle. As Fig. 1 points out, $F_p = 5$ produces relatively no distortion in the peripheries compared to $F_p = 10$. Therefore, $F_p = 5$ will be used hereafter to avoid the effect of the calibration error whereas the view angle is restricted to 136°.

B. Sun Positioning

The solar forecasting process mainly relies on the position of the sun in the sky images, which is accurately indicated and updated over successive time intervals. Scanning the sky image for the brightest area does not work perfectly in practice as optically thin clouds can be intensely illuminated by the sun and considerably deviate the sun-locating process. Therefore, a computational approach is deployed, which yields the angular position of the sun corresponding to the specific geographic information, date and time [24]. The fish-eye coordinates of the sun is obtained and then translated into undistorted coordinates using the calibration toolbox.

Fig. 1. (a) Sample fish-eye photo of a checkerboard and the undistorted images. (b) $F_p = 5$. (c) $F_p = 10$.

C. Cloud Segmentation

Different optical properties of atmospheric aerosols and constituent particles of the clouds create a relatively marked visual distinction between clear and cloudy regions of the sky. RBR value of each pixel has proven to be an effective approach to generate the cloud mask by discriminating the cloud pixels from the clear sky [25]. However, applying an ordinary thresholding on the RBR value of the pixels usually shows an unreliable performance in different regions of the sky. This is mainly attributed to the nonuniform luminance pattern of the sky due to the scattering effect of atmosphere on the sun beams [26], which is also shown in Fig. 2(d). This effect can be compensated by comparing the real-time sky image against the corresponding clear sky reference (CSR) image in RBR values. The resulting differential array is then thresholded by Θ_{RBR} to identify the cloud areas. For this purpose, the sun position (zenith and azimuth angle) in the CSR has to be aligned with that of the real-time sky image. Therefore, a collection of clear sky images is created, where each element corresponds to a specific zenith angle considering the daily and seasonal variations of the sun trajectory. It ranges from minimum zenith angle of 7° at high noon on the summer solstice in Perth, Australia, to the maximum of 70° that corresponds to the extreme zenith angles at the start and end of the prediction algorithm at sunrise and sunset times, respectively. Moreover, each element of the clear sky collection (CSC) is center rotated so that the sun is aligned to the azimuth angle of zero. This allows instant reconstruction of the CSR respective to any angular position of the sun; the element closest to the real-time zenith angle of the sun is chosen and center rotated by its azimuth angle. To prevent computational burden, the sky image and the respective CSR are undistorted and averaged block-wise and the corresponding RBR value is calculated for each block instead of pixel-wise processing. Fig. 2(c) and (f) illustrate the RBR images of the real-time sky view and the associated CSR represented in false color, respectively. The resulting differential image is illustrated in Fig. 2(g) which is thresholded to identify the cloud regions. The cutting value of Θ_{RBR} is tuned practically through observations and a satisfactory cloud detection process is achieved by the value of 0.176, as shown in Fig. 2(h). The thresholding process produces a binary cloud mask representing the clear sky in *zero* and clouds in *one*. The shape of the clouds is then defined in a sequence of the coordinates on the outline of the respective area termed as "contours," which is illustrated in Fig. 2(i). Although, the CSR differentiation relatively avoids the severe illumination rise in the circumsolar area the cloud detection in this region is comparatively unreliable and only useful for relatively short-term subminute prediction range, e.g., 1 min. Therefore, for longer prediction ranges, i.e., 10 min, the circumsolar area can be subtracted from the initially detected clouds. This operation is achieved by scattering the contours into small hexagons and those overlapped the circumsolar area are excluded, purple contours in Fig. 2(j).

D. Cloud Motion

The motion analysis of the observed clouds is a significant component of the prediction method. An optical-flow approach is deployed to identify the motion of the objects between two successive frames. It calculates an array of two-dimensional displacement vectors respective to all pixels or blocks of pixels [27]. The vectors are then filtered by the binary cloud mask Fig. 2(h) to obtain the motion elements of the pixels inside the cloud regions. Fig. 2(j) gives an example of the motion vectors resulting from two successive samples. Using a simplifying assumption that all visible clouds are single layer making a uniform motion in a horizontal plane, the instantaneous velocity vector $\vec{V}(t_0)$ is obtained by averaging the validated collection of motion vectors

$$\vec{V}(t_0) = \frac{1}{t_c} \sum_{i=1}^{n} \frac{\vec{d}_i}{n} \tag{1}$$

where t_0 and t_c are sampling instant and cycling time of the algorithm, respectively, over which n displacement values of $\vec{d}_1$ through $\vec{d}_n$ have been observed. Afterward, to smooth out the turbulent movement of the clouds or any occasional passing object within effective view of the camera, previous instantaneous motions corresponding to three recent cycles ($r = 3$) of the algorithm are averaged to obtain the principal velocity vector $\bar{\vec{V}}(t_0)$, which is introduced into the forecasting section of the proposed algorithm.

$$\bar{\vec{V}}(t_0) = \frac{1}{r} \sum_{i=0}^{r} \vec{V}(t_0 - i \cdot t_c). \tag{2}$$

To ease the deployment of observation data for future predictions, in each cycle an observation structure containing the

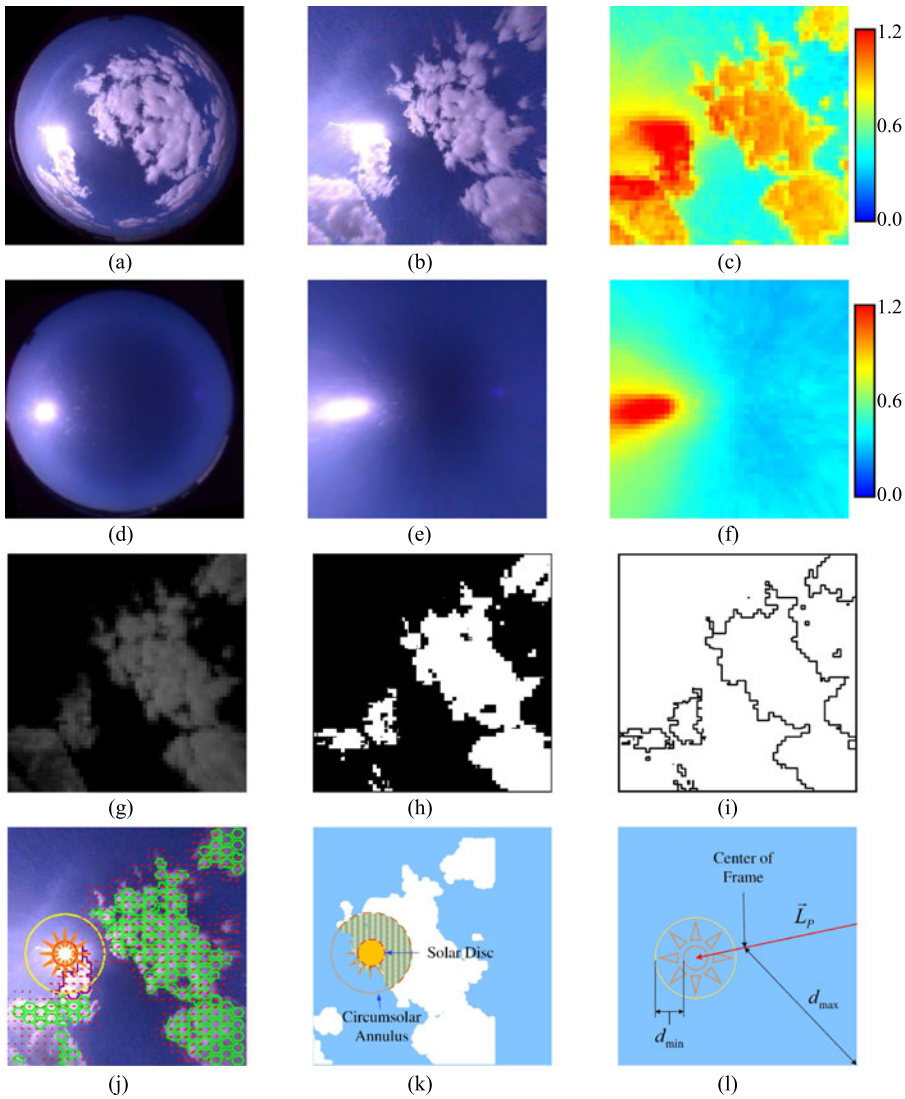

Fig. 2. Real-time captured image (a) fish-eye, (b) undistorted, (c) RBR in false color. Reconstructed clear sky image, (d) fish-eye, (e) undistorted, (f) RBR in false color. Cloud segmentation, (g) differential image, (h) thresholded by Θ_{RBR}, (i) cloud contours. (j) Cloud motion. (k) Cloud Forecast. (l) Observation ranges and effective range of displacement prediction.

associated time tag t_r, cloud mask, and principal velocity vector is created as follows:

$$\mathrm{obs}(t_r) = \begin{cases} \text{reference time:} & t_r \\ \text{cloud outline:} & C \\ \text{velocity vector:} & \bar{\vec{V}}(t_r). \end{cases} \tag{3}$$

E. Cloud Forecasting

Given the key assumption of the persistent movement of the clouds, the projected displacement value of $\vec{D}_{t_0}^{t_1}$, associated with a time interval of t_0 to t_1, is obtained by extrapolating the principal velocity vector from the time origin.

$$\vec{D}_{t_0}^{t_1} = \bar{\vec{V}}(t_0) \times (t_1 - t_0). \tag{4}$$

In order to make a more reliable prediction, which is less susceptible to occasional errors in segmentation and optical-flow, a series of historical observations are incorporated. Respective to each prediction time t_f a suitable range for the reference time of historic observation is defined as follows:

$$t_0 + t_f - t_{h2} < t_r < t_0 + t_f - t_{h1}. \tag{5}$$

Given the cloud segments neighboring the solar area are projected to create a shade in the very close future, eliminating the circumsolar clouds in the segmentation stage and the very short-term cloud prediction is omitted. Therefore, the historic observations closer than t_{h1} to the target prediction time $t_0 + t_f$ does not contain useful cloud information and have to be excluded in the forecasting process. Moreover, due to the limited effective prediction range (viewing angle of the camera) the outdated observations spaced back farther than t_{h2} prior to the target prediction time $t_0 + t_f$ are projected out of the observation plane and have to be disregarded as well. Both t_{h1} and t_{h2} could be experimentally obtained

$$t_{h1} = d_{\min}/V_{\mathrm{avg}} \tag{6}$$

$$t_{h2} = d_{\max}/V_{\mathrm{avg}} \tag{7}$$

where V_{avg} is the average motion amplitude over the available historic information, e.g., few months, recorded as 0.46 pix/s. Hence, $d_{\min} = 55$ pix is the circumsolar distance and $d_{\max} = 339$ pix is the longest radius of the frame as shown in Fig. 2(l). Therefore, it gives $t_{h1} \approx 120$ s and $t_{h2} \approx 755$ s. Afterward, the cloud outlines respective to the eligible observations (5) are displaced according to (4). A mean predicted cloud outline is then generated from the collection of the displaced cloud outlines, which are then averaged pixel-wise and normalized to [0–255] to produce a single monochrome image. This image is then thresholded by the middle intensity value of $\Theta_{\text{avg}} = 256 \div 2 = 128$ to generate the averaged predicted cloud outline. Fig. 2(k) shows the result of the averaged prediction process as a binary cloud mask, which is overlayed onto the solar disc templates to obtain the predicted cloudiness indexes. The solar disc template consists of a circle equal in size to the sun as observed in the undistorted image and centered on the calculated coordinate of the sun. The pixel count of the projected cloud mask that overlaps the solar disc template (highlighted in yellow) is then normalized by the solar disc area to produce the respective solar occlusion index, SOi, which is a fair indication of the predicted attenuation of solar insolation. Similarly, a circumsolar template is an annulus with an inner radius equal to the size of the solar disc, and an outer radius twice that size. The circumsolar occlusion index, COi, is the normalized conjunction of the circumsolar annulus and the cloud mask (highlighted in green), which could be interpreted as a moderate likelihood of sunlight obstruction in future time. However, when it comes to fast moving intermittent clouds, it is more challenging to predict a shading event that is occurring relatively far away from current time. The effective prediction range, T_P, is defined as the time a cloud segment takes to travel the effective displacement prediction, $\vec{L}_P$, at the velocity and orientation of the observed principal motion. As shown in Fig. 2(l), $\vec{L}_P$ is the shortest trajectory from the margin of viewing field to the position of the sun.

$$T_P = |\vec{L}_P|/|\bar{\vec{V}}(t_0)|. \tag{8}$$

Hence, the cloud prediction algorithm is capable of indicating occlusion of the sun for a prediction time up to the effective range and fails when that time exceeds T_p. This is a motivation for proposing multipoint forecasting, as opposed to a single target, in which prediction is performed at a series of evenly spaced prediction instants

$$\{t_0 + t_{\text{sp}},\ t_0 + 2 \cdot t_{\text{sp}},\ \ldots\ ,\ t_0 + n \cdot t_{\text{sp}}\} \tag{9}$$

$$n \times t_{\text{sp}} = t_f \tag{10}$$

where t_f and t_{sp} are total and split forecast ranges, respectively. Moreover, n stands for the total number of prediction instants. This is a solution to address the all-or-nothing nature of the individual target prediction, i.e., a shading event out of an effective range will be still identified prior to its occurrence yet not at a perfect time. Therefore, pointing to a specific time forward, the multipoint prediction generates a series of SOi and COi values corresponding to the elements of prediction time series as per (9).

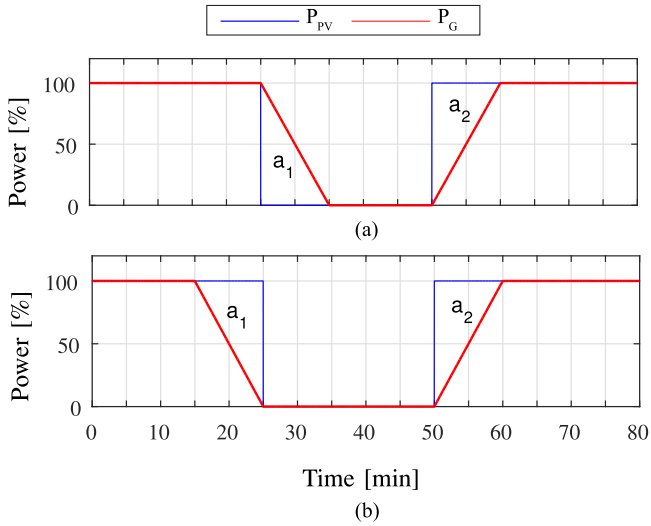

Fig. 3. Energy balance in PVG smoothing. (a) Conventional smoothing. (b) Based on cloud prediction.

III. Proposed PVG Smoothing Approach

For grid-tied PVG systems compliance with operators RR requirements, i.e., 10% per minute RR tolerance as per [2], ensures that grid is not disturbed and power quality criteria are satisfied. Sudden under/over generation of a PV plant primarily attributed to passing clouds and their shading characteristics can be addressed in different ways. This section outlines the conventional nonpredictive approach followed by cloud prediction aided proactive strategies. In the end, a new battery-less smoothing technique using conservative cloud prediction by the sky-camera is explained.

A. Conventional Nonpredictive Smoothing Strategy

This method works on the assumption that the PV plant is continuously operating at its maximum power point (MPP), while the generation is monitored and undue RR is compensated by means of a backup storage device such as BS. Equations (11)–(13) elucidate how the ramp function defines the PVG export power.

$$R(t_0) = \frac{P_{\text{PV}}(t_0) - P_G(t_0 - t_s)}{t_s} \tag{11}$$

$$R_r(t_0) = \begin{cases} R_s & \text{if } R(t_0) > R_s \\ -R_s & \text{if } R(t_0) < -R_s \\ R(t_0) & \text{otherwise .} \end{cases} \tag{12}$$

$$P_G(t_0) = P_G(t_0 - t_s) + R_r(t_0 - t_s) \times t_s \tag{13}$$

where P_{PV} and P_G are PV plant generation and the resulting smoothed power, respectively. t_0 and t_S stand for present time and sampling rate, respectively. Moreover, R and R_s represent instantaneous RR of the PVG and the associated extreme allowable RR, respectively.

Fig. 3(a) depicts an nonpredictive smoothing process over a sudden 100% drop in the generation follows the full recovery. The upward and downward ramp functions are initiated upon

the detection of sudden changes. During the ramp down period, the deficit energy marked by a_1 has to be injected while ramp-up smoothing requires energy absorption equal to area a_2. This explains the critical role of a storage device such as BS of sufficient capacity to ensure an acceptable nonpredictive PVG regulation. Given the upward ramps could be simply yet not utmost efficiently compensated by curtailment of the surplus power instead of energy absorption, battery-less PVG regulation is technically viable provided the ramp down procedures are started sufficiently prior to the occurrence of the PVG under generation period. This requires an algorithm that accurately predicts the timing and amplitude of sudden under generations caused by passing clouds. Fig. 3(b) illustrates the battery-less predictive regulation and as seen it only involves energy curtailment. Therefore, the mitigation of the storage does not disrupt the smoothing function.

In the following section, cloud prediction information is incorporated to the conventional smoothing algorithm to investigate whether a satisfactory storage-free smoothing approach is achieved, given the limitations and relative deficiencies of the imagery-based cloud prediction methods.

B. Ideal Export Prediction Smoothing Strategy

Smoothing approach purely based on prediction is ideally defined on the assumption that valid projected PVG output is available all the time. The required prediction range t_f is inversely proportional to the maximum allowable RR.

$$t_f = 1/R_s. \tag{14}$$

Equations (15)–(16) are applied to all projection points within the prediction range in order to generate the most critical RR and the appropriately restricted ramp for PVG is determined by (17):

$$R_i(t_0) = \frac{P_P(t_i) - P_G(t_0)}{t_i - t_0} \; i \in (1:n) \tag{15}$$

$$R_c(t_0) = \min\{R_1(t_0),\ R_2(t_0), \ldots,\ R_n(t_0)\} \tag{16}$$

$$R_r(t_0) = \begin{cases} R_s & \text{if } R_c(t_0) > R_s \\ -R_s & \text{if } R_c(t_0) < -R_s \\ R_c(t_0) & \text{otherwise} \end{cases} \tag{17}$$

$$P_G(t_0) = P_G(t_0 - t_s) + R_c(t_0 - t_s) \times t_s \tag{18}$$

where $R_i(t_0)$ is the required RR to bridge the present PVG value $P_G(t_0)$ to the expected generation level at the ith prediction point $P_P(t_i)$ and n is the number of prediction instants. Moreover, $R_c(t_0)$ is the most critical RR, which has to be followed in order to achieve a smooth P_G only by allowing energy curtailment and without any back up power injection. R_s and $R_r(t_0)$ are the extreme allowed RR and the RR command to the PV system, respectively. The plant export power is eventually defined by (18).

A practical storage-less PVG smoothing approach requires a precise prediction of P_{PV} by estimating the solar insolation, incidence angle, and temperature of the PV panels. Any inaccuracy arising from prediction process might need supporting power injection to compensate that. Alternatively, the lack of desired precision could be appropriately addressed to mitigate the required storage backup. In the following sections, two different attempts to develop a prediction-based PVG output smoothing approach are examined and compared in their effectiveness and functionality.

C. Proposed Smoothing Method-I: Using Output Estimation

The principle of this approach is to estimate the projected solar insolation according to the predicted cloudiness indices. Therefore, based on the specifications of the test system, we make few simplifying assumptions; virtually constant open-circuit voltage V_{OC}, PV panel temperature T, and fill-factor of FF. This results in the generated power being proportional to insolation S

$$\begin{aligned} &P_{\text{MPP}} = \text{FF} \cdot V_{\text{OC}} \cdot I_{\text{SC}} \\ &I_{\text{SC}} \propto S \text{ at } T = 25^{\circ} \\ &V_{\text{OC}} = 388.8[V] = \text{cte},\ \ \text{FF} = 0.73 = \text{cte} \\ &\therefore P_{\text{MPP}} \propto S \end{aligned} \tag{19}$$

where I_{SC} and P_{MPP} signify the short-circuit current and PV power at MPP, respectively. Furthermore, the angle of incident for the direct component of the solar irradiance can be obtained using the coordinates of the sun generated by the solar positioning procedure [24] and alignment of the PV array. Therefore, a rough approximation of P_{PV} forecast values, $P_P(t_i)$, are obtained in (20)

$$P_P(t_i) = P_{\text{MPP}}(t_i) = P_{\text{STC}} \cdot \cos(\alpha) \cdot \text{SO}i \tag{20}$$

where P_{STC} is the PVG output in standard test conditions (STC), α is the solar incident angle, and SOi is the respective solar occlusion factor. The simplified estimation of (20) is used to obtain the projected generation values, $P_P(t_i)$, and the governing principle of the ideal prediction, (15)–(18), are applied to meet the appropriate RR requirement. As the smoothing control primarily relies on sudden variations, rather than precise estimation of the export power of the PV plant, in spite of the applied simplifications and resultant inaccuracies the prediction information effectively improved the smoothing process in terms of required backup power.

D. Proposed Method-II: Smoothing Using Binary Cloud Prediction

In order to address the limitations discussed earlier with respect to the PVG output estimation, a conservative PVG export smoothing strategy based on a binary cloud prediction is proposed. This proactive approach slowly lowers the export power into a reduced value during the critical situations when it is highly likely that solar occlusion occurs and ramps that up when the clouds are passed. This is determined by the projected cloudiness figures SOi and COi. Therefore, the projected plant

export power at the prediction range is defined by (21).

$$P_P(t_f) = \begin{cases} P_{\text{Base}} & \text{if } \sum \text{SO}i > \Theta_{\text{SO}} \\ P_{\text{Base}} & \text{if } \sum \text{CO}i > \Theta_{\text{CO}} \\ P_{\text{MPP}} & \text{otherwise} \end{cases} \tag{21}$$

where Θ_{SO} and Θ_{CO} are threshold values associated with aggregated SOi and COi values, respectively. Furthermore, P_{Base} is the target amount of generated power during shut-off condition, which is determined as a percentage of the nominal amount of expected generation in clear sky condition at the time ($P_{\text{STC}} \cdot \cos(\alpha)$). The transmissivity characteristic of the obscuring clouds is a decisive factor in subsequent incident radiation, which barely causes the PVG output to decline by more than 75%–80% [28]. Hence, the shut-off coefficient of C_{Base} is assigned a value of 20%, which enables efficient utilisation of the PVG yield while smooth power generation is maintained

$$P_{\text{Base}}(t) = C_{\text{Base}} \cdot P_{\text{STC}} \cdot \cos(\alpha). \tag{22}$$

The projected export value $P_P(t_f)$ is then introduced to (15)–(18) to determine the respective reference export power.

IV. Developed Testbed and Experimental Setup

This section sets out the configuration of hardware components of the testbed developed for conducting a series of evaluative trials on the proposed PVG smoothing approach. The key component of the developed system is a weather proof fish-eye security camera with a wide dynamic range (WDR) to accommodate the extremely broad extent of pixel brightness in the sky image, ranging from the sun disc to relatively dark cloud regions, without a considerable level of saturation in the image. The IP camera is mounted upright facing the sky in an outdoor area and communicated through local area network (LAN). Based on the proposed strategy discussed in Section III-D a cloud prediction software is developed and implemented on a Linux operating Raspberry Pi computer, which acquires snapshots from the sky camera in regular time steps and then generates and archives recent cloud segmentation and optical flow data used for the solar occlusion forecast. Meanwhile, for the purpose of future analysis all key data are logged, i.e., image processing results, SOi and COi figures. Ultimately, the RR command is generated and sent out to a solar-gate [29], which is an intermediate device to enable external control of the PV power export by overriding the maximum power point tracking (MPPT) operation of the grid-tied solar inverter #1. The solar inverter #2 is used with no export smoothing control to allow a comparative evaluation of the proposed PVG smoothing algorithm. Fig. 4 makes a visual presentation of the composition of the testbed while Table I gives further details about that.

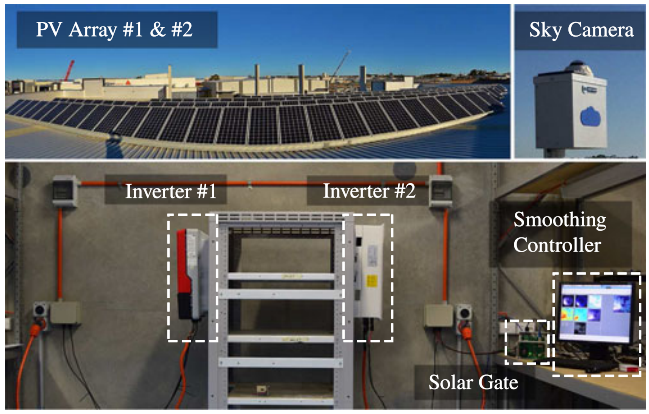

Fig. 4. Photo of the testbed for PVG smoothing based on the proposed cloud prediction technique.

TABLE I
Specifications of Testbed

	Parameter	Value
Camera	Model	ACTi E925
	Communication	TCP/IP
	Viewing Angle	189°(overview), 115.3°(high detail)
	Focal Length	Fixed, f1.19 mm
	Dynamic Range	Basic WDR 74 dB
Controller	Model	Raspberry Pi 2 Model B
	CPU	900 MHz quad-core ARM Cortex-A7
	RAM	1 GB
	Storage	16 GB
Inverter #1	Model	SMA Sunny Boy 5000TL
	Rated power	4.6 kW
	Nominal AC voltage	210–230 V
	MPP voltage range	100–500 V
	Max. input current	15 A
Inverter #2	Model	Solis-4K-2G
	Rated power	4 kVA
	Nominal AC voltage	180–270 V
	MPP voltage range	100–500 V
	Max. input current	15 A
PV Array #1 / #2	Module	ESM200S-125 Monocrystalline
	Open Circuit Voltage-V_{OC}	388.8 V
	Short Circuit Current-I_{SC}	6.3 A
	Peak Power Watts-P_{MPP}	1.8 kW @ 314.1 V , 5.73 A
	Panel Azimuth Angle	0 °N
	Panel Tilt Angle	34°
Location	Latitude	32.1 °S
	Longitude	115.81 °E
	Elevation	31 m

V. Evaluation and Analysis

This section aims at establishing a benchmark to assess performance and eligibility of the previously discussed PVG smoothing schemes. Those are compared with the nonpredictive method in terms of required capacity of the storage backup and the frequency of its usage. A preliminary trial experiment was conducted at Magellan Power in Western Australia, including different meteorological conditions, i.e., fully sunny, overcast, and partly cloudy. The collected data set include all the critical prediction data including SOi, COi, incident angle α, and the export power of the uncontrolled solar inverters #2. It allows trying different set points of (21) on the simulation model of the proposed PVG smoothing algorithm in MATLAB/Simulink to obtain the most suitable values. The lowest the cutting values Θ_{SO} and Θ_{CO} are, the more sensitive and conservative becomes the proposed cloud prediction algorithm. The optimized values of $\Theta_{\text{SO}} = 0.15$ and $\Theta_{\text{CO}} = 0.15$ ensure the best performance so

TABLE II
SMOOTHING SET POINTS

Parameter	Symbol	Value
Permissible RR	R_s	180 Wmin^{-1}
Min Observation Range	t_{h1}	120 s
Max Observation Range	t_{h2}	155 s
Forecast Range	t_f	10 min
Split Forecast Range	t_{sp}	30 s
SOi Threshold	Θ_{SO}	0.15
COi Threshold	Θ_{CO}	0.15
Shut-Off Coefficient	C_{Base}	20%

that almost all of the cloud events are detected properly. Further reduction and narrowing down the threshold values will not offer significant improvement in the prediction quality, but tend to create occasional erroneous ramp down commands during the clear sky periods. Afterwards, an evaluative trial was also carried out over ten days in December 2015 to demonstrate the practical viability of the proposed smoothing algorithm. The 10 min prediction range is chosen according to the desired RR of 10% per minute. In this experiment, inverter #1 was subject to the export smoothing based on the proposed binary prediction approach of Section III-D and the set points in Table II. Concurrently, inverter #2 was connected to the same size of PV array and operating normally at MPP with no smoothing controls and the critical real-time information is logged to provide the actual PVG data for the purpose of simulating the other smoothing approaches in exactly the same weather condition as the practical test of the proposed binary prediction approach. The simulation models of the other smoothing approaches are also developed in MATLAB/Simulink to conduct a comparative study. As representative samples, the measurement results of the proposed binary cloud prediction based PVG smoothing approach are presented accompanied with the simulation results associated with the other methods using the nonpredictive approach, ideal export prediction, and output estimation. Figs. 5 and 7 illustrate the comparative results for December 4 and 8, 2015, with scattered fast-moving clouds, and mostly clear sky, respectively. Furthermore, the aggregated SOi and COi figures and the resultant smoothing command are illustrated in Figs. 6 and 8, respectively. The energy balance profile, i.e., energy yield, smoothing power injection, and absorption for different approaches are summarised and compared in Fig. 9. To allow a more valid comparison it is assumed that the absorbed energy is not recovered into the grid while the injected energy is supplied to meet the RR criteria.

As discussed in Section III and indicated by (13) and (18), in the smoothing process the plant export power is governed so as to satisfy the RR requirements. Therefore, the sudden variations of the generated power have to be treated by a storage system such as BS of sufficient energy and power capacity. Incorporating the cloud prediction information, depending on how early the sudden variations are predicted and how accurately the projected PVG level is estimated, tends to mitigate the reliance on the required power injection (see Fig. 3).

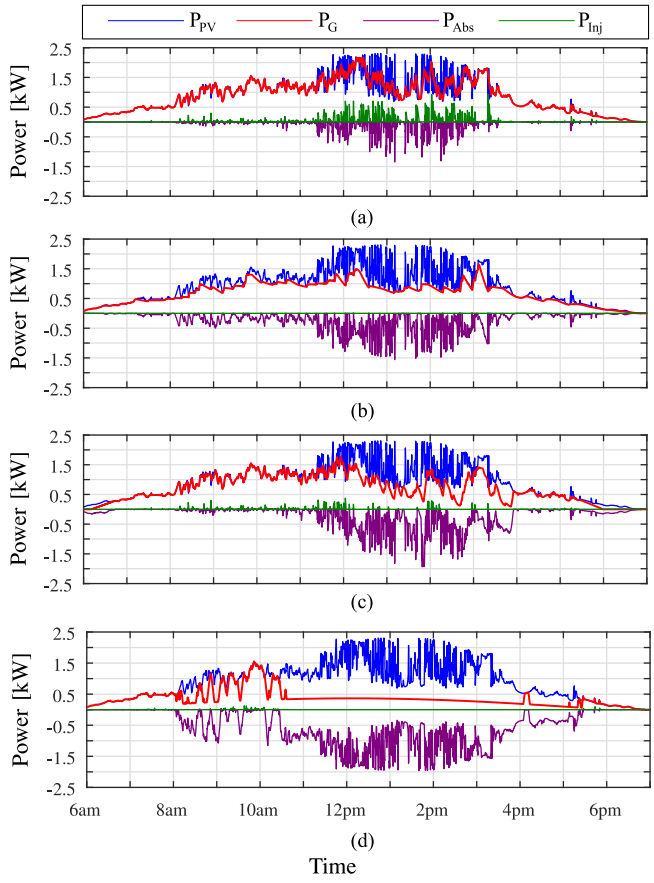

Fig. 5. Smoothing results for December 4, 2015. (a) Nonpredictive. (b) Ideal Prediction. (c) Estimation based. (d) Binary Prediction.

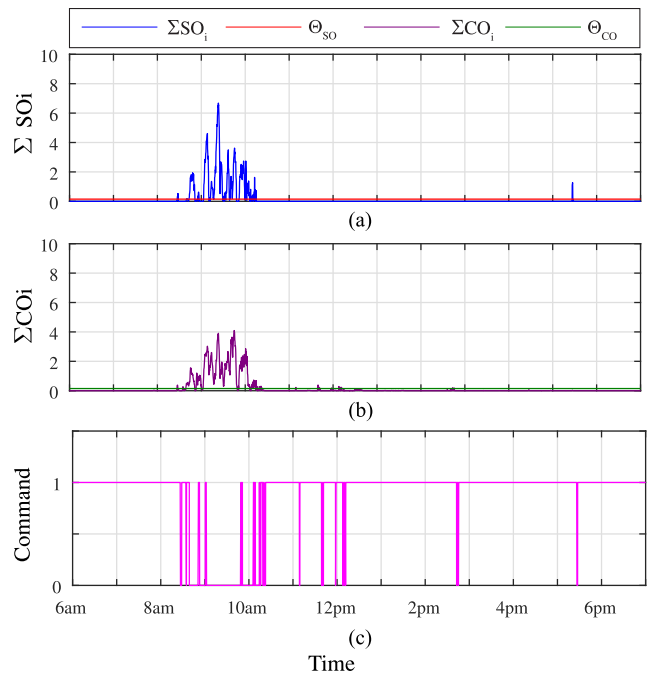

Fig. 6. Smoothing signals for December 4, 2015. (a) Total SOi. (b) Total COi. (c) Export toggle command to solar inverter #1.

The following remarks could be concluded from the comparative results.

1) The nonpredictive PVG smoothing [Section III-A; (11)–(13)] involves bidirectional supporting energy exchange during ramp events. Therefore, energy injection and absorption on ramp down and ramp up processes, respectively, are essential to maintain the RR requirement. This is illustrated in Figs. 5(a) and 7(a) where P_{Inj} and P_{Abs} represent the injected and absorbed power, respectively. Therefore, the storage support is inevitable in this approach, which is a financial impediment to vast deployment of PV resources across the areas that RR requirement is a precondition for grid integration of PVG plants. In particular not all battery technologies are capable of delivering a cycle time as short as 10 min, as the typical power density normally allows around 1hr cycling time [30]. Hence, the BS has to be oversized in energy capacity to meet the power density of smoothing treatment. On the other hand, as Fig. 9(a) shows this approach exhibits a relatively high energy efficiency due to relatively less energy absorption. Nevertheless, the capital cost and the maintenance of BS have created a motivation for exploring more economical alternatives.
2) As Figs. 5(b) and 7(b) imply, the ideal export prediction PVG smoothing [Section III-B; (15)–(18)] shifts the direction of smoothing energy exchange toward the absorption and it no longer involves power injection. Fig. 9(b) also confirms the fact that the energy injection could be totally mitigated provided the accurate prediction information determines the occurrence of the under/over generations and the resulting PV export power is precisely estimated. However, the utmost yield is achieved when the storage is deployed to handle the energy absorption P_{Abs} and deliver that slowly into the utility grid, meanwhile maintaining the RR requirement. Moreover, the unidirectional smoothing power allows for possible elimination of the storage at the cost of reduced energy efficiency of the smoothing process, as indicated in Fig. 9(a). The financial benefit of mitigating the storage distinctly outweighs the reduced financial revenue due to the lower yield. The capital price of the BS system normally accounts for a significant portion of the total cost of a BS assisted PV plant, e.g., it adds up to 50% to price of the PVG plant, as of 2012 in U.S. [31]. Considering that, Perth, Western Australia, in average has only 30% cloudy days a year [32]. Given, the cloudy days are not of high yield compared to an ordinary sunny day and only a portion of the generation is curtailed in the smoothing process. The BS can recover less than 30% of annual yield while requiring up to 50% additional capital investment, which is not financially justified compared to the prediction-based PVG smoothing approach.
3) The proposed PVG smoothing based on output estimation [Section III-C; (19)–(20)] shows virtually varying performance depending on the degree of cloudiness. As seen in Figs. 5(c) and 7(c) this method suffers from the

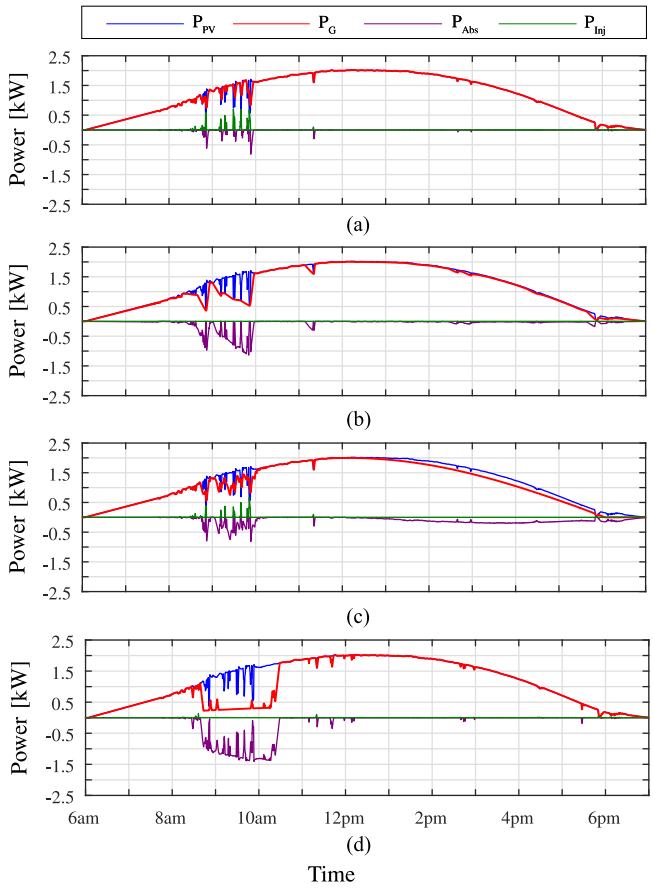

Fig. 7. Smoothing results for December 8, 2015. (a) Nonpredictive. (b) Ideal Prediction. (c) Estimation based. (d) Binary Prediction.

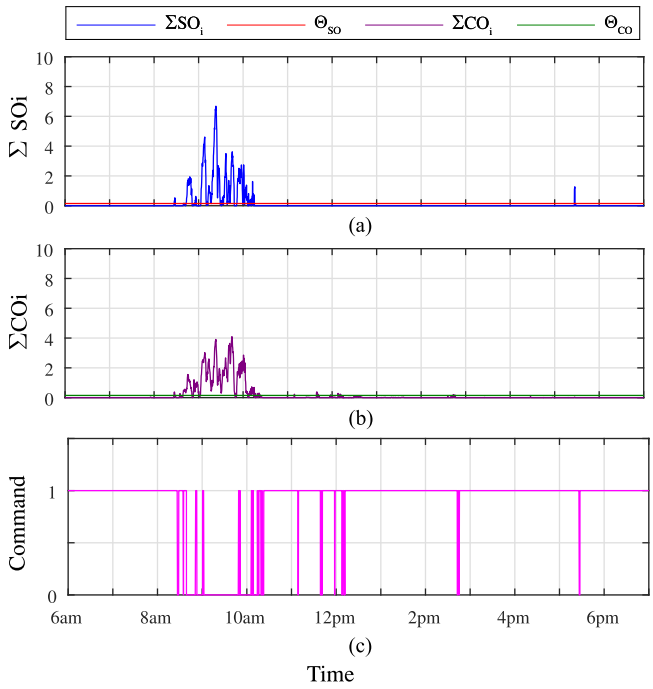

Fig. 8. Smoothing signals for December 8, 2015. (a) Total SOi. (b) Total COi. (c) Export toggle command to solar inverter #1.

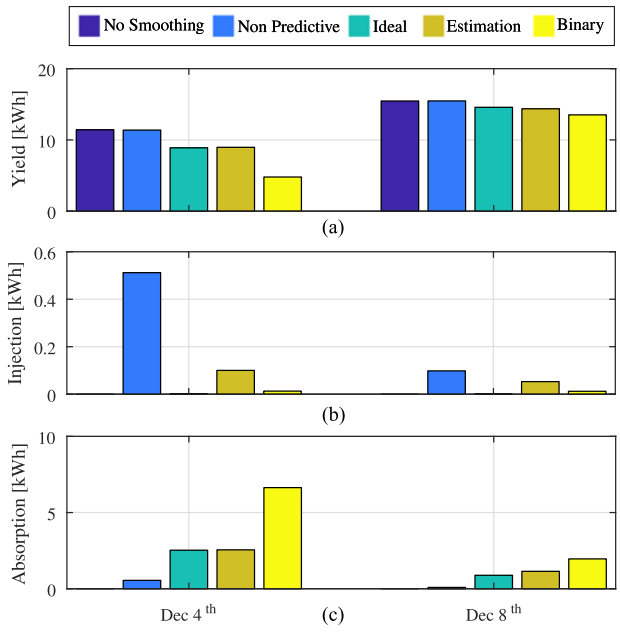

Fig. 9. Segregated energy balance for different smoothing approaches. (a) Energy yield. (b) Injected energy. (c) Absorbed energy.

lack of perfect accuracy in the presence of fast moving clouds. This is a typical drawback to the imagery-based cloud prediction approaches. On the other hand, in highly cloudy days with substantially intermittent generation level, even a relatively inaccurate forecast makes a remarkable decrease in the energy and power injection backup for the smoothing. In contrast, in the case of occasional brief shadings on a mostly sunny day it fails to make a significant reduction in the smoothing energy injection either in terms of power, or occurrence frequency [see Fig. 9(b)]. This is mainly attributed to the estimation error during clear-sky periods. Moreover, the simplifications made in the calculation of projected generation level in (19) creates an offset estimation error during the clear sky periods and unnecessary energy absorption [see Fig. 7(c)]. Therefore, the output estimation method exhibits a relatively inferior energy yield compared to the ideal export prediction [Fig. 9(a)]. Although it reduces the amount of injected smoothing energy, this smoothing approach involves bidirectional energy exchange, which still makes the assistance of the storage unavoidable.

4) The proposed binary prediction based PVG smoothing approach [Section III-D; (21)–(22)], in essence, operates on the principle that the PVG export power is restricted once passing clouds are projected to obscure the solar disc or the circumsolar region. This conservative solution compensates for the inherent imperfect accuracy of the cloud prediction process. Regardless of the magnitude of the projected export reduction, output power slowly ramps down to a reduced amount P_{Base}, which will not be affected by the coming shading event. Hence, a reduced energy harvest only during the cloudy days is typical of this approach compared to the ideal PVG export prediction [see Fig. 9(a)]. The simulation results suggest that during the passing clouds this method needs an inconsiderable amount of backup power injection P_{Inj} in only a very few instances a day, which is negligible when compared with the conventional nonpredictive method (Figs. 5 and 7). In practice, slight deviations from the required RR up to a certain extent is allowed by most network operators, e.g., the Horizon Power Corporation in Western Australia permits for a 10% nonlinearity in the RR of PVG power export [33]. The experimental results show that the supporting power exchange never exceeded the allowed nonlinearity band ($10\% \times 1.8 = 0.18$ kW) that can be well accommodated by the existing spinning reserves of the utility grid. From the financial point of view, a justification similar to the ideal prediction method holds for the practical proposed binary cloud prediction method as well. Therefore, given the minimum energy efficiency in the worst case scenario, the proposed binary cloud prediction method still exhibits a better financial profile compared to the conventional nonpredictive BS-based approach.

VI. Conclusion

This paper proposes a predictive approach regulating the erratic PVG export variations attributed to the passing clouds to mitigate the extra burden on the operational reserve capacity of the utility grid. This smoothing method works on the principle of initiating a ramp down function sufficiently prior to the appearance of passing clouds over the PV array. Compared to the nonpredictive approaches that react to the PVG intermittency issues upon the incidence, in the proposed method the sudden and disruptive PVG export variations are mostly avoided and the reliance on the backup power injection is significantly reduced accordingly. This highlights the *proactive* characteristics of the proposed smoothing approach as opposed to the *reactive* nature of the nonpredictive solutions. The performance and practical viability of the proposed method are evaluated through a series of experimental tests on a prototype constructed at Magellan Power in Western Australia. The experimental results are also compared with the associated results of the conventional nonpredictive smoothing strategy simulated in MATLAB/Simulink. The main conclusions are as follows.

1) A perfectly accurate PVG output prediction enables a regulation method with no reliance on the back-up power injection while the amount of produced energy is not remarkably compromised.
2) Given the inherent shortcomings of the imagery-based prediction approaches, a novel averaged cloud prediction scheme with improved robustness is proposed that is capable of indicating the erratic solar generation variations sufficiently ahead of its incidence.
3) The proposed binary cloud prediction using a sky camera could significantly mitigate the reliance of the conventional PVG smoothing strategy on the supporting power injection.

4) However due to the conservative nature of the cloud prediction algorithm, for some operating conditions the approach may suffer from an inferior energy harvest profile when compared with the ideal prediction technique.
5) In the case of the proposed binary prediction based method, the financial benefit of mitigating storage support well outweighs the curtailed energy involves during the passing clouds.
6) The experimental outcomes of the proposed prediction assisted PVG smoothing method support the feasibility of a reliable battery-less RR smoothing solution.

REFERENCES

[1] E. Ela, M. Milligan, and B. Kirby, "Operating reserves and variable generation," Nat. Renew. Energy Lab., Golden, CO, USA, Rep. NREL/TP-5500-51978, Aug. 2011.

[2] V. Gevorgian and S. Booth, "Review of PREPA technical requirements for interconnecting wind and solar generation," Nat. Renew. Energy Lab., Rep., Golden, CO, USA, Rep. NREL/TP-5D00-57089, Nov. 2013.

[3] "National Electricity Rules Version 79," Australian Energy Market Commission (AEMC), Sydney, NSW, Australia, Mar. 2016.

[4] "Interconnection Requirements for Variable Generation," North American Electric Reliability Corporation (NERC), Atlanta, GA, USA, 2012, Art. no. 121.

[5] M. Bragard, N. Soltau, S. Thomas, and R. W. De Doncker, "The balance of renewable sources and user demands in Grids: Power electronics for modular battery energy storage systems," *IEEE Trans. Power Electron.*, vol. 25, no. 12, pp. 3049–3056, Dec. 2010.

[6] O. M. Toledoa, D. O. Filhoa, and A. S. A. C. Dinizb, "Distributed PV generation and energy storage Systems: A review," *Renew. Sustain. Energy Rev.*, vol. 14, no. 1, Jan. 2010, Art. no. 506511.

[7] J. Tant, F. Geth, D. Six, P. Tant, and J. Driesen, "Multiobjective battery storage to improve PV integration in residential distribution grids," *IEEE Trans. Sustain. Energy*, vol. 4, no. 1, pp. 182–191, Jan. 2013.

[8] J. Marcos, O. Storkl, L. Marroyo, M. Garcia, and E. Lorenzo, "Storage requirements for PV power ramp-rate control," *Solar Energy*, vol. 99, pp. 28–35, Jun. 2014.

[9] M. J. E. Alam, K. M. Muttaqi, and D. Sutanto, "Mitigation of rooftop solar PV impacts and evening peak support by managing available capacity of distributed energy storage systems," *IEEE Trans. Power Syst.*, vol. 28, no. 4, pp. 3874–3884, Nov. 2013.

[10] M. J. E. Alam, K. M. Muttaqi, and D. Sutanto, "A novel approach for ramp-rate control of solar PV using energy storage to mitigate output fluctuations caused by cloud passing," *IEEE Trans. Energy Convers.*, vol. 29, no. 2, pp. 507–518, Jun. 2014.

[11] A. M. Gee, F. V. P. Robinson, and R. W. Dunn, "Analysis of battery lifetime extension in a small-scale wind-energy system using supercapacitors," *IEEE Trans. Energy Convers.*, vol. 28, no. 1, pp. 24–33, Mar. 2013.

[12] H. Zhou, T. Bhattacharya, T. Duong, T. S. T. Siew, and A. M. Khambadkone, "Composite energy storage system involving battery and ultracapacitor with dynamic energy management in microgrid applications," *IEEE Trans. Power Electron.*, vol. 26, no. 3, pp. 923–930, Mar. 2011.

[13] Seung-TakKim and J.-W. Park, "Energy management strategy and adaptive control for SMES in power system with a PV Farm," *J. Electr. Eng. Technol.*, vol. 9, pp. 742–747, 2014.

[14] Z. Wang, Z. Zou, and Y. Zheng, "Design and control of a photovoltaic energy and SMES hybrid system with current-source grid inverter," *IEEE Trans. Sustain. Energy*, vol. 4, no. 2, pp. 464–473, Jun. 2013.

[15] R. Naik, N. Mohan, M. Rogers, and A. Bulawka, "A novel grid interface, optimized for utility-scale applications of photovoltaic, wind-electric, and fuel-cell systems," *IEEE Trans. Power Del.*, vol. 10, no. 4, pp. 1920–1926, Oct. 1995.

[16] F. Capp, M. Lazarewicz, A. Arseneaux, P. Dresens, and H. Rojas, "Methods, systems and apparatus for regulating frequency of generated power using flywheel energy storage systems with varying load and/or power generation," U.S. Patent 8,008,804, Aug. 2011. [Online]. Available: http://www.google.com/patents/US8008804

[17] M. Diagne, M. David, P. Lauret, J. Boland, and N. Schmutz, "Review of solar irradiance forecasting methods and a proposition for small-scale insular grids," *Renew. Sustain. Energy Rev.*, vol. 27, pp. 65–76, Nov. 2013.

[18] C. W. Chow *et al.*, "Intra-hour forecasting with a total sky imager at the UC san diego solar energy testbed," *Solar Energy*, vol. 85, no. 11, pp. 2881–2893, Nov. 2011.

[19] B. Urquhart, M. Ghonima, D. Nguyen, B. Kurtz, C. W. Chow, and J. Kleissl, "Sky-imaging systems for short-term forecasting," in *Solar Energy Forecasting and Resource Assessment*, J. Kleissl, Ed. Boston, MA, USA: Academic, 2013, ch. 9, pp. 195–232.

[20] H. Yang *et al.*, "Solar irradiance forecasting using a ground-based sky imager developed at UC san diego," *Solar Energy*, vol. 103, pp. 502–524, May 2014.

[21] S. R. West, D. Rowe, S. Sayeef, and A. Berry, "Short-term irradiance forecasting using Skycams: Motivation and development," *Solar Energy*, vol. 110, pp. 188–207, Dec. 2014.

[22] D. Bernecker, C. Riess, E. Angelopoulou, and J. Hornegger, "Continuous short-term irradiance forecasts using sky images," *Solar Energy*, vol. 110, pp. 303–315, Dec. 2014.

[23] D. Scaramuzza, A. Martinelli, and R. Siegwart, "A toolbox for easily calibrating omnidirectional cameras," in *IEEE/RSJ Int. Conf. Intell. Robots Syst.*, Oct. 2006, pp. 5695–5701.

[24] I. Reda and A. Andreas, "Solar position algorithm for solar radiation applications," *Solar Energy*, vol. 76, no. 5, pp. 577–589, 2004.

[25] R. W. Johnson, W. S. Hering, and J. E. Shields, "Automated visibility & cloud cover measurements with a solid state imaging system," Scripps Institution of Oceanography, University of California, San Diego, CA, USA, Rep. MPL-U-26/89, 1989.

[26] R. Kittler, M. Kocifaj, and S. Darula, "Propagation of light in the atmospheric environment," in *Daylight Science and Daylighting Technology*. New York, NY, USA: Springer-Verlag, 2012, ch. 4, pp. 97–125.

[27] R. Szeliski, "Dense Motion Estimation," in *Computer Vision: Algorithms and Applications*. New York, NY, USA: Springer-Verlag, 2010, ch. 8, p. 812.

[28] M. Paulescu, E. Paulescu, P. Gravila, and V. Badescu, "The future of the energy mix paradigm," in *Weather Modeling and Forecasting of PV Systems Operation* (Green Energy and Technology), J. Kleissl, Ed. London, U.K.: Springer-Verlag, 2013, ch. 1, pp. 1–15.

[29] "Magellan Solar Export Control Solutions Solar Gate," Magellan Power, 2015, p. 8. [Online]. Available: http://magellanpower.com.au/Products/Renewable-Energy-and-Energy-Storag e-Systems/Solar-Gate

[30] National Research Council, *Meeting the Energy Needs of Future Warriors*. Washington, DC, USA: The National Academies Press, 2004. [Online]. Available: http://www.nap.edu/catalog/11065/meeting-the-energy-needs-of-future-war riors

[31] "Solar Photovoltaics," in *Renewable Energy Technologies(Cost Analysis Series)*. Abu Dhabi, UAE: The International Renewable Energy Agency (IRENA), 2012, p. 21, volume 1:Power Sector, Issue 4/5.

[32] Bureau of Meteorology. Climate Statistics for Australian Sites, 2016. [Online]. Available: http://www.bom.gov.au/climate/data/

[33] "Technical Requirements for Renewable Energy Systems Connected to the Low Voltage (LV) Network via Inverters," HPC-9FJ-12-0001-2012, Horizon Power Corporation, WA, Australia, 2012, p. 58. [Online]. Available: http://horizonpower.com.au/media/1121/technical-requirements-for-renewable-energy-systems-connected-to-the-low-voltage-lv-network-via-inverters.pdf

Mojtaba Saleh (S'10) received the B.Sc. degree in electronics engineering from the University of Isfahan, Isfahan, Iran, and the M.Sc. degree in electrical engineering from Iran University of Science and Technology (IUST), Tehran, Iran, in 2008 and 2011, respectively. He is currently working toward the Ph.D. degree in electrical engineering at Curtin University, Perth, WA, Australia.

From 2009 to 2011, he was a Research Student in Power Electronic and Electric, Magnetic Fields Research Laboratory, IUST. He joined Magellan Powertronics as an R&D Engineer in 2013. His main research interests include modeling, design and control of power electronic converters, renewable energy resources, and battery storage systems.

Lindsay Meek (M'91) was born in Christchurch, New Zealand, in 1970. He received the B.Eng. degree in computer systems from Curtin University, Perth, WA, Australia, in 1991, and the M.Phil. degree in Physics from Murdoch University, Perth, WA, Australia, in 1994.

He is the Chief Technology Officer at Magellan Powertronics, and has worked as an R&D Engineer in the power electronics industry for the past 20 years. During this time has published several papers and magazine articles, and completed more than 100 R&D projects.

Mr. Meek has received several awards and placings in design innovation contests, including the Horizon Innovation Challenge, the NASA design the future contest, the Shell innovation challenge, and four major prizes from international electronic design contests.

Mohammad A. S. Masoum (S'88–M'91–SM'05) received the B.S. and M.S. degrees from the University of Colorado, Denver, CO, USA, in 1883, 1985; respectively, and the Ph.D. degree from the University of Colorado, Boulder, CO, USA, in 1991 all in electrical and computer engineering.

He is the Program Leader for Sustainable Power Systems within the Centre for Smart Grid and Sustainable Power Systems and a Professor at the Department of Electrical and Computer Engineering, Curtin University, Perth, WA, Australia. He has published more than 100 journal articles and 200 conference papers. He is the co-author of Power Quality in Power Systems and Electrical Machines (Elsevier, 2008 and 2015) and Power Conversion of Renewable Energy Systems (Springer, 2011 and 2012).

Dr. Masoum is a Editor of the IEEE TRANSACTIONS ON SMART GRID and IEEE POWER ENGINEERING LETTERS, Guest Editor of the IEEE TRANSACTIONS ON INDUSTRIAL INFORMATICS, and Editor of *Australian Journal of Electrical and Electronic Engineering*.

Masoud Abshar received the M.Sc. degree in power electronics engineering from Loughborough University, England, U.K., in 1982.

He is the founder and the current Managing Director of Magellan Powertronics Pty Ltd, a Western Australian Power Electronics Manufacturing company. He is a Chartered Engineer with 35 years experience and regularly speaks at events and conferences on Power Electronics and Energy Storage. Magellan Powertronics specialises in customised DC and AC backup power equipment and in the past 26 years has been supplying its products to some of Australia's biggest industrial projects. For the past decade, Mr Abshar and his Research and Development team at Magellan have been working on innovative Renewable Energy and Energy Storage solutions.